Transition metal adatom and dimer adsorbed on graphene: Induced magnetization and electronic structures

Chao Cao,[1,2,*] Min Wu,[2] Jianzhong Jiang,[2] and Hai-Ping Cheng[3]
[1]*Department of Physics, Hangzhou Normal University, Hangzhou 310036, People's Republic of China*
[2]*International Center for New Structured Materials (ICNSM), Laboratory of New Structured Materials (LNSM), Department of Materials Science and Engineering, Zhejiang University, Hangzhou 310013, People's Republic of China*
[3]*Quantum Theory Project and Department of Physics, University of Florida, Gainesville, Florida 32611, USA*
(Received 10 October 2009; revised manuscript received 24 March 2010; published 17 May 2010)

Geometries, electronic structures, and magnetic properties of transition metal M adatom and dimer adsorbed graphene have been studied (M=Fe, Co, Ni, and Cu). With adatom adsorption, we confirm the previously reported stable adsorption site, and the adatoms are chemically bonded with graphene except the copper adatom. With dimer adsorption, we observed that the stable configurations are dependent on the exchange-correlation functional for the iron dimer and nickel dimer; while the stable configurations do not depend on the functional for the cobalt and copper dimer. The adsorption energy indicates the copper dimer can barrierlessly diffuse along the graphene C-C bonds. With iron or cobalt adatom adsorption, graphene becomes a half-metal which can be used as a spin-filtering material. The iron dimer adsorbed graphene is also a half-metal, but the cobalt dimer adsorbed graphene is not. Both local-density approximation and generalized gradient approximation yield consistent results for the nickel adatom adsorbed graphene, which is the system is semiconducting and nonmagnetic due to the strong binding between nickel and graphene. However, different exchange-correlation functionals lead to controversial results for the magnetic and transport properties of nickel dimer adsorbed graphene. The copper adatom adsorbed on graphene exhibits $1\mu_B$ local magnetic moment, but the dimer does not show any magnetism. These results show that graphene properties can be effectively modulated by transition metal adsorption and that the transition metal adsorbed graphene can serve as potential materials in nanoelectronics, spintronics, or electrochemistry.

DOI: 10.1103/PhysRevB.81.205424 PACS number(s): 73.22.−f, 61.48.De, 73.20.At

I. INTRODUCTION

Graphene, a type of carbon based material, has attracted great attention from both experimentalists and theoretists since its experimental discovery in 2004.[1] Structurally, graphene consists of a single-layer graphite sheet, thus the electrons are restricted to the atomic thin sheet, forming two-dimensional electron gas (2DEG). It has been found that the material is a zero-gap semiconductor and that its band energy dispersion is linear around the Fermi level E_F.[2] Therefore, the electrons around E_F can be regarded as two-dimensional massless Dirac fermions with substitution of speed of light c by its Fermi velocity v_F. As a result, graphene is of great interest to fundamental studies as a workbench for quantum electrodynamics (QED). A typical example is the anomalous integer quantum hall effect (QHE) of the massless Dirac fermion.

Graphene is also regarded as a potential material for future electronics due to its extremely long mean-free path and thus stimulates the studies on the defects and impurities. Hashimoto *et al.* experimentally studied the monovacancy, multivacancy, and Stone-Wales vacancy on graphene.[3] Son *et al.* studied the edge states of graphene nanoribbons (GNR), and found that the edge state of zigzag GNR is antiferromagnetic (AFM) with an energy gap.[4,5] Williams *et al.* realized *p-n* junction on graphene and studied its conductivity and QHE experimentally,[6] and Abanin *et al.* made theoretical explanation using model Hamiltonians.[7] Based on the theoretical studies about the transport properties of electron doped graphene by Hwang *et al.*,[8] Schedin *et al.* performed experiments showing that the *n*-doped graphene can be used as good sensors of gas molecules.[9] Huang *et al.* and Wehling *et al.* then took out theoretical studies on this issue.[10]

Among the vast amount of studies on graphene, transition metal cluster adsorption on graphene is relatively less studied. Theoretically, Che *et al.* carefully examined the interface between graphene and Pd/Pt surfaces, and explained the different behavior between the palladium-graphene interface and the platinum-graphene interface.[11] Vanin *et al.* then studied the transition metal-graphene interfaces using the Van der Waals corrected density functionals.[12] Khomyakov *et al.* also studied the interactions and charge transfers between graphene and various metal surfaces.[13] Karpan *et al.* performed calculations on the interface between graphene and the close-packed surfaces of nickel or cobalt, and predicted spin-filtering effect.[14] Duffy and Blackman investigated the magnetism of transition metal adatoms and dimers on graphite long before graphene was discovered.[15] Chan *et al.* performed density-functional calculations and studied metal adatom adsorption on graphene.[16] Although these calculations claimed chemisorption of transition metal clusters on graphene, Johll *et al.* claimed physisorption of transition metal clusters on graphene.[17] Besides, Duffy *et al.* and Johll *et al.* found different stable configurations for the metal dimers adsorption on graphene. These calculations mainly focused on the geometric properties and energetics. Wu *et al.* studied the copper adatom and dimer adsorption on graphene from the first principles.[18] More recently, Wehling *et al.* performed *ab initio* calculations on Co adatoms on graphene, and identified an orbitally controlled Kondo effect.[19] Longo

et al. studied Fe_n and Ni_n clusters ($n=1$ 4) adsorbed on hydrogen passivated graphene nanoribbons;[20] while Rigo *et al.* studied the electronic structure and transport properties of Ni_n cluster doped graphene nanoribbons.[21] Similar systems were also investigated by Sevinçli*et al.*[22] Üzengi Aktürk *et al.* studied noble-metal clusters Au_n and Pt_n adsorption on graphene using the first-principles calculations.[23] Sanchez-Paisal *et al.* also studied Zr_n clusters adsorption and diffusion properties on graphene.[24] Using *ab initio* calculations, Choi *et al.* proposed to employ natural carbon-nitrogen-transition metal complexes to disperse hydrogen-adsorbing transition metals on a large scale.[25] Experimentally, the studies of transition metal clusters are very difficult, and thus most experimental studies are performed on transition metal surfaces and graphene.[26,27]

The rest of the paper is organized as follows: in the next section, we briefly discuss the model and parameters used in our calculations; then we present our calculation results of single adatom adsorption, and dimer adsorption in separated subsections, combined with detailed discussions; and finally, we summarize our results and draw the conclusion.

II. METHOD AND CALCULATION DETAILS

We employed density-functional theory (DFT) as implemented in PWSCF in the QUANTUM-ESPRESSO package to model our systems.[28] In order to model a metal adatom or dimer adsorbed on single graphene layer, we chose a 7×7 supercell of graphene, i.e., 98 carbon atoms plus one adatom or dimer in the simulation cell. In the direction perpendicular to the graphene plane, a 15 Å inter-graphene-layer distance was used to eliminate the interactions between the neighboring images. In all calculations, a set of plane-wave basis up to 36 Ry was used, and the augmented charge density energy cutoff was chosen to be 400 Ry.[29] The local spin-density approximation (LSDA) to the exchange-correlation functional generally yields worse energetic properties, geometric structure, as well as magnetic properties; but the generalized gradient approximations (GGAs) are known to fail for weakly bonded (van der Waals) systems such as graphene and graphite. Since there is no obvious suitable choice of the exchange-correlation functional, we modeled the exchange-correlation energies with the LSDA parametrized by Perdew and Zunger[30] as well as the GGA parametrized by Perdew, Burke, and Ernzerhof.[31] The first Brillouin zone was sampled with $3\times3\times1\Gamma$-centered special grid, and the density of states was obtained with $12\times12\times1\Gamma$-centered grid and a Gaussian smearing of 0.1 eV. The graphene lattice constant was obtained by varying the perfect graphene lattice, which turned out to be 1.42 and 1.43 Å in LSDA and PBE calculations, respectively. The transition-metal-adsorbed graphene structures were carefully optimized until the maximum force is less than 0.001 Ry/bohr and the total energy difference is smaller than 1 meV. During the optimization, all internal coordinates including the adsorbed atoms and the carbon atoms were allowed to be relaxed, while the lattice constants were kept fixed.

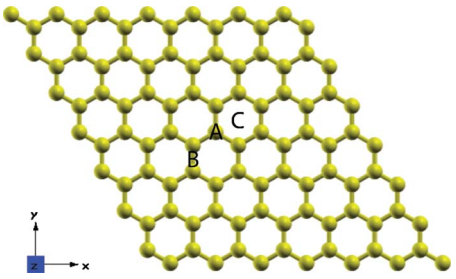

FIG. 1. (Color online) Possible adsorption sites of a single adatom onto single-layer graphene. "*A*" is right above a carbon atom (atom-top site); "*B*" is right above the middle of a C-C bond (bond-top site); and "*C*" is right above the center of the hexagonal (hex-center site).

III. RESULTS AND DISCUSSION

A. Single adatom adsorption

Because of the hexagonal symmetry of the graphene lattice, possible adsorption sites for a single atom can be reduced into three types: the atom-top site, the bond-top site, and hex-center site (Fig. 1). We list our results for a metal adatom adsorbed on graphene in Table I. The LDA and PBE results are consistent for all four types of systems. The iron, cobalt and nickel adatoms are strongly bonded to the hex-center site, except for the copper adatom, which is relatively weakly bonded to the bond-center site. For the adsorption energies (E_{ad}) of the iron, cobalt, and nickel adatoms, our results are similar to those obtained by Duffy *et al.*[15] (LDA results) and Yagi *et al.*[32] (GGA results), and are significantly higher than those reported by Johll *et al.*[17] (PBE results). The

TABLE I. The optimized structure and binding energies of single adatom adsorbed on graphene layer. $h_M=z_M-\overline{z_C}$, where $\overline{z_C}$ is averaged over all carbon atoms. $d_{M\text{-}C}$ is the averaged bond length of the metal atom and the nearest carbon atoms. E_{ad} is the adatom adsorption energy defined as $E_{ad}=E_M+E_{graphene}-E_{tot}$, in unit of eV/atom; and m_{cell} is the magnetic moment per unit cell, in the unit of μ_B. The values outside the parenthesis are PBE results, and the values inside the parenthesis are LSDA results.

Atom	Site	h_M (Å)	$d_{M\text{-}C}$ (Å)	E_{ad} (eV)	m_{cell} (μ_B)
Fe	H	1.44(1.50)	2.11(2.06)	1.06(2.20)	2.13(2.44)
Co	H	1.46(1.47)	2.10(2.04)	2.08(3.25)	1.43(1.13)
Ni	H	1.49(1.55)	2.11(2.06)	2.79(3.94)	0.00(0.00)
Cu	B	2.04(2.16)	2.20(2.07)	0.44(0.85)	0.64(0.56)

major difference between our LDA results and those from Duffy *et al.* is that their calculations employed the linear combination of atomic orbitals (LCAO) and we used the plane-wave basis set. The difference between our results and those from Johll *et al.* may come from different choice of isolated metal-atom configurations. The free metal atomic configurations (electron occupancies) we employed (Fe:$3d^6 4s^2$, Co:$3d^7 4s^2$, Ni:$3d^8 4s^2$, Cu:$3d^{10} 4s^1$) are different from what they used (Fe:$3d^{6.32} 4s^{1.64}$, Co:$3d^{7.62} 4s^{1.36}$, Ni:$3d^{8.77} 4s^{1.23}$). Johll *et al.* proposed that the second argument to be most probable. We varied the electron occupancies of the free metal atoms, and it turns out that the lowest configuration energies for Fe($3d^{6.2} s^{1.8}$), Co($3d^{7.7} 4s^{1.3}$), and Ni($3d^{9.0} 4s^{1.0}$) are 0.05, 0.47, and 1.20 eV lower than the EM values we used to calculate E_{ad}. All four types of M-C bonds have similar bond lengths from 2.04 to 2.07 Å under LDA; while under PBE, the Cu-C bond length is about 5% larger than those of Fe-C, Co-C, and Ni-C. The bond lengths and binding energies indicate that the iron, cobalt, and nickel adatoms are chemically bonded with the graphene sheet; and the copper adatom is physisorbed on graphene. The adsorption energy for copper adatom is significantly lower than that reported by Wu *et al.* because the spin correction was not correctly taken into consideration in the previous calculation.[18]

The ground state of the iron/cobalt adatom adsorbed graphene inevitably shows local magnetism around the metal adatoms as expected (Table I). Surprisingly, the nickel atom, which normally shows magnetism at bulk states, shows no magnetism when it is adsorbed on graphene. Spin-polarized calculations with both ferromagnetic (FM) and antiferromagnetic (AFM) initial guess (with a 2×1 supercell) converge to the nonmagnetic (NM) state. To the contrary of nickel atom, the copper atom shows about $0.5\mu_B$/cell magnetism.

In order to further analyze the electronic structure and related properties of the transition metal adatom adsorbed graphene, we first performed the projected density of states (PDOS) calculations for these systems. Both LDA and PBE functionals yield very similar result, therefore we show only the PBE results in Fig. 2. Despite of the low concentration of the transition metal adsorbed ($\approx$1% as the number percentage), these metal atoms modify the graphene electronic structure drastically. For the iron and the cobalt adatom adsorbed systems, their DOS open a gap of approximately 0.2 eV for the majority spin, but remain continuous for the minority spin. Therefore, both the iron and the cobalt adatom adsorbed graphene are expected to be good spin-filtering materials as reported.[14,33] For the nickel adsorbed system, the strong metal-carbon binding completely destroys the delocalized π orbital of the graphene layer, and the system open a small gap of 0.1 eV at the Fermi level. It is well known that the gap sizes are generally underestimated with DFT calculations, the material is therefore expected to be a semiconductor. The copper adsorbed system shows continuous DOS around E_F for both spins, but at E_F the DOS of majority spin reaches the peak while the DOS of minority spin is almost zero. Finally, the PDOS calculations show that for the copper adsorbed system, Cu 4s orbitals dominate the majority spin states around E_F; for the iron and cobalt adsorbed systems, M 3d (M=Fe,Co) orbitals dominate the minority spin states around E_F; and for the nickel adsorbed system, Ni 3d orbitals dominate the states around E_F.

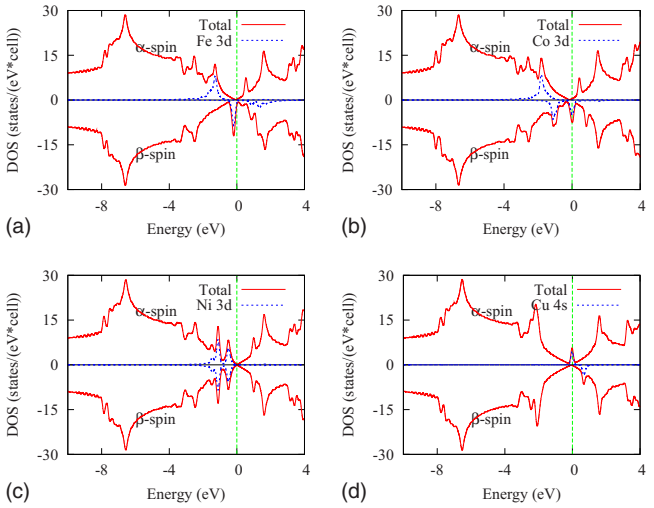

FIG. 2. (Color online) Electronic density of states projected onto atomic orbitals of the adatom. For Fe, Co, and Ni, the chosen orbitals are M 3d; for Cu, the chosen orbital is Cu 4s. The solid lines are total DOS; dotted lines are PDOS of the chosen adatom atomic orbitals. Upper panels present α spin (the majority spin); and the lower panels are β spin (the minority spin).

PDOS calculations also yield Löwdin's charge information. Due to the restrictions of the used pseudopotentials, where no p-orbital information for the transition metal atoms was presented, all calculations reported zero contribution from the p orbitals of the transition metal atoms. Nevertheless, for all the metal atoms investigated, no more than 0.8e charge transfer was observed (Table II), showing that the M-C bonds are of covalent nature. For the iron atom adsorbed on graphene, a charge transfer from its 4s orbital to 3d orbitals occurs due to the orbital hybridizations, leaving $\approx 2e$ electrons unpaired and thus yielding $2\mu_B$ magnetic moment. The same argument applies to both cobalt (one unpaired electron) and nickel (no unpaired electron) atoms adsorbed on graphene. For the copper atom adsorbed on graphene, the 4s electron cannot be transferred to the full 3d shell of copper atom, thus the unpaired electron is of s character (Table II).

B. Metal dimer adsorption

The dimer cluster adsorption forms more complex structure than the adatom adsorption does (Fig. 3). On one hand, the dimer can either lie *parallel* to the graphene layer, and both atoms form equally strong binding with graphene; or one of the atoms can be substantially closer to the graphene layer than the other, forming a *tilted* dimer on graphene; or more likely the dimer almost stands *vertically* toward the graphene layer, and effectively the dimer binds to graphene only through the lower atom. On the other hand, the lower atom (or both atoms in the parallel case) can bind to three different sites as discussed in previous subsection. In our calculations, we considered six possible initial configurations (Fig. 3), and the final configurations were obtained by opti-

TABLE II. Charge analysis and local magnetic moment on the transition metal atom. "valence" refers to the valence electron configuration for a neutral atom as in its pseudopotential file; n_M to the Löwdin's charge of the atom; m_{atom} to the local magnetic moment on the transition metal adatom; m_s the magnetic moment contribution from the transition metal s orbitals. The numbers outside the parenthesis are the PBE results, and the numbers inside the parenthesis are the LDA results. The difference between the number of neutral valence electrons and the Löwdin's charge is regarded as the number of electrons transferred.

Atom	Valence	n_M	$n_{M\ 3d}$	m_{atom} (μ_B)	m_s (μ_B)
Fe	$3d^6 4s^2$	7.31(7.38)	7.16(7.23)	2.21(2.00)	−0.01(−0.01)
Co	$3d^7 4s^2$	8.40(8.45)	8.25(8.30)	1.19(0.99)	0.00(0.00)
Ni	$3d^8 4s^2$	9.30(9.24)	9.13(9.07)	0.00(0.00)	0.00(0.00)
Cu	$3d^{10} 4s^1$	10.87(10.87)	9.85(9.84)	0.86(0.85)	0.84(0.83)

mizing the initial configurations. Before the structural optimization, the dimer atoms were slightly displaced (≈0.01 Å) away from the high symmetry sites (atom-top, bond-top, hex-center) to avoid the local minima. It is worthy noting that after full optimization, the dimer atoms might deviate from these high symmetry sites, and the notations just indicate the closest final configurations. However, large deviation is only observed in the PBE calculation of Fe C_v configuration, whose optimized structure is shown in Fig. 3(d). We list the structural optimization results for all four dimer adsorbed graphene systems in Table III, and detailed discussions are presented in the following subsections.

1. Fe-dimer adsorbed graphene

For the iron-dimer adsorbed graphene, the LDA and PBE calculations yield very different results. In LDA calculations, the iron-dimer atoms do not favor the hex-center site as the iron adatom does, and are adsorbed at two bond-center sites, forming a B_h configuration (Table III). The two Fe atoms are therefore equivalent in this configuration. In PBE calculations, however, the iron dimer is not adsorbed at any high symmetry site [Fig. 3(d)]. The Fe atom close to graphene (Fe^1) has appreciably deviated away from the hex-center site, and forms a bond of 2.21 Å with one of the carbon atoms. The angle formed by this Fe^1-C bond and the norm of the

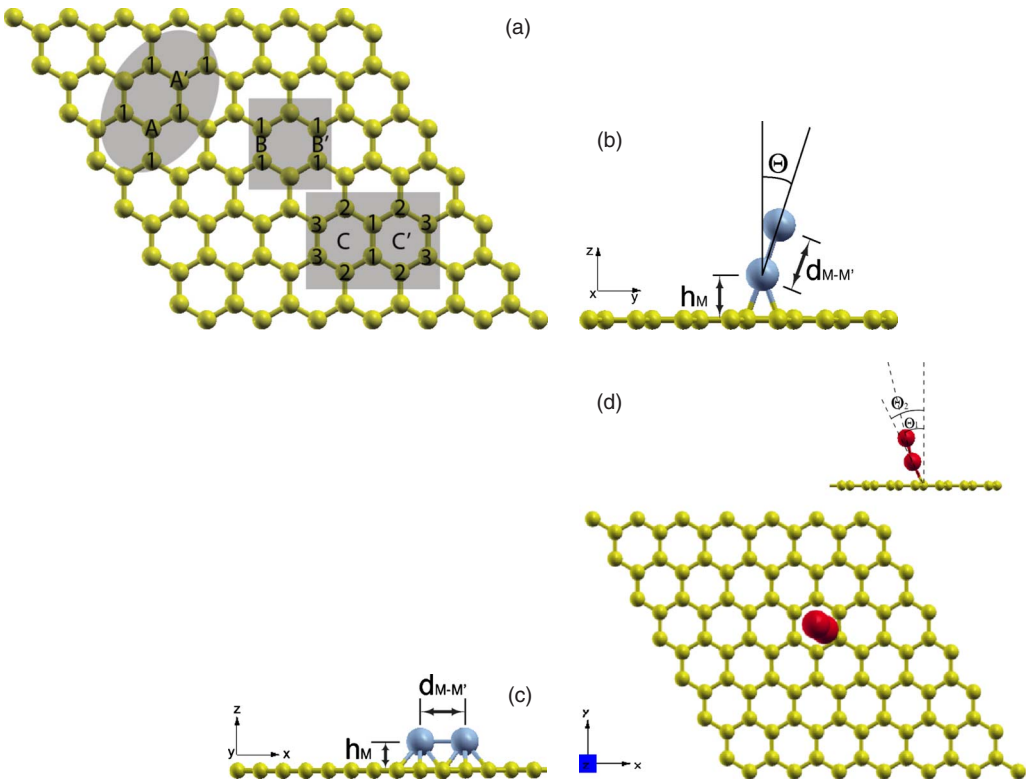

FIG. 3. (Color online) Possible adsorption sites of a dimer on a single-layer graphene. (1) The dimer stands almost perpendicular to the graphene layer. The lower atom is bonded to either (a) atom-top, (b) bond-top, or (c) hex-center site. These configurations are referred to as A_v, B_v, and C_v, respectively, in this paper. (2) The dimer lies parallel to the graphene layer. The two atoms are binded to S and S'' [S =(a) atom-top, (b) bond-top, or (c) hex-center] sites, respectively. These configurations are referred to as A_h, B_h, and C_h, respectively, in this paper. The left-top shadowed area is an example of an A_h configuration; the middle shadowed area is an example of a B_h configuration; and the right-bottom shadowed area is an example of a C_h configuration.

TABLE III. The optimized structure and binding energies of metal dimer adsorption on graphene layer. E_{conf} refers to the relative energy of a specific configuration to the stable one, which is indicated by 0 in bold font. $h_M = z_M - \overline{z_C}$, where $\overline{z_C}$ is averaged over all carbon atoms, and M is the metal atom closer to the graphene layer. Θ is the angle formed by the dimer and the norm of the graphene sheet, as illustrated in Fig. 3(b). $d_{M\text{-}C}$ is the averaged bond length of the metal atom and the nearest carbon atoms. $d_{M\text{-}M'}$ is the M-M' distance as in the dimer-graphene complex, and the number in the parenthesis is the bond length as in an isolated dimer. E_{ad} is the dimer adsorption energy defined as $E_{ad}=E_{dimer}+E_{graphene}-E_{tot}$ in unit of eV/dimer, and the number in the parenthesis is the binding energy of an isolated dimer defined as $E_b=2\times E_M-E_{dimer}$. m_{cell} is the magnetic moment per unit cell in the unit of μ_B, and the number in the parenthesis is the magnetic moment for an isolated dimer. The notation "to S_s" indicates that after the relaxation, the original symmetry of the initial configuration was completely eliminated, and the structure simultaneously transform into another configuration S_s.

		E_{conf} (meV/cell)						h_M	Θ	$d_{M\text{-}C}$	$d_{M\text{-}M'}$	$E_{ad}(E_b)$	m_{cell}
	Atom	A_v	B_v	C_v	A_h	B_h	C_h	(Å)	(°)	(Å)	(Å)	(eV)	(μ_B)
PBE	Fe	59	19	**0**[a]	to B_h	269	374	2.02	25.66	2.21	2.07(1.96)	0.77(3.19)	6.46(6.00)
	Co	to C_v	to C_v	**0**	to B_h	617	to B_h	1.72	1.84	2.21	2.06(1.95)	1.13(4.73)	3.99(4.00)
	Ni	183	to C_v	**0**	to B_h	225	226	1.75	0.95	2.25	2.14(2.08)	0.92(5.44)	2.04(2.00)
	Cu	31	**0**	145	398	397	to B_v	2.21	6.23	2.20	2.20(2.26)	0.43(2.53)	0.00(0.00)
LDA	Fe	169	337	171	to B_h	**0**	101	191		2.04	2.01(1.89)	1.67(4.06)	6.00(6.00)
	Co	567	to C_v	**0**	179	179	259	1.64	2.36	2.14	1.97(1.87)	1.91(5.56)	3.96(4.00)
	Ni	1046	1444	1129	to C_h	to C_h	**0**	1.53		2.10	2.36(2.04)	2.53(5.98)	0.00(2.00)
	Cu	5	**0**	133	305	349	to A_v	2.03	4.24	2.08	2.21(2.19)	1.08(2.62)	0.00(0.00)

[a]Under PBE calculations, iron-dimer adsorbed graphene does not take high symmetry configuration after relaxation. We will discuss its structure in detail in context.

graphene plane (Θ_2) turns out to be 25.40°. Due to the binding between the Fe^1 atom and the graphene sheet, the dimer bond is weakened, as the bond length increases by ≈5%. The dimer bond also tilts and forms an angle (Θ_1) of 15.18° with the norm of the graphene plane. This result has been verified using different pseudopotentials, and even in a different plane-wave code (VASP) using projected augmented wave (PAW) method. The calculations confirmed that the most stable configuration of iron-dimer adsorbed graphene depends on the exchange-correlation functional employed in the calculation, and thus a simple density-functional calculation is not capable to determine the structure of this system. Our PBE results are also in consistent with those obtained by Johll *et al.*[17]

Since LDA and PBE leads to different stable configurations, the DOS of the system are also very different in LDA and PBE. However, the difference in the DOS are mostly due to the different stable configurations obtained since the DOS are very similar if one compares them for the same configuration in either LDA or PBE. Despite of the very different DOS shapes, the iron-dimer adsorbed graphene is also a half-metal in both LDA and PBE calculations since the DOS shows an energy gap of ≈0.25 eV (0.1 eV) for the majority spin channel in PBE (LDA) calculations and no energy gap for the minority spin channel (Fig. 4). In LDA calculations, the two Fe atoms are equivalent due to the C_{2v} symmetry of the system, and the PDOS of them are exactly the same. In PBE calculations, the Fe atom closer to the graphene layer is labeled as Fe^1, and the other Fe atom is labeled as Fe^2. The PDOS analysis shows that, in both calculations, the Fe 3*d* orbitals and C 2*p* orbitals dominate the states from $E_F-4.0$ eV to $E_F+2.0$ eV, and they strongly hybridize for the minority spin from approximately $E_F-1.8$ eV to $E_F+1.8$ eV and for the majority spin from $E_F-4.0$ eV to E_F.

We also performed the Löwdin's charge analysis, and the results are listed in Table IV. In LDA calculations, the two equivalent iron atoms lose only $0.34e$/atom, showing the covalent character of the bondings. Each iron atom possesses ≈7 electrons on its five 3*d* orbitals after the orbital hybridizations, thus three electrons remain unpaired and the local magnetism of the iron atom is $3\mu_B$. Calculation shows that an isolated iron dimer also has a magnetic moment of $6\mu_B$. In PBE calculations, the iron dimer very weakly binds with the graphene sheet through Fe^1 atom, thus Fe^1 atom loses ≈0.2 electrons while Fe^2 atom remains almost neutral. The Fe^1 and Fe^2 atoms possess ≈7.0 and 6.7 electrons, respectively. They yields approximately 3 unpaired electrons each, and therefore the total magnetic moment is $6.46\mu_B$/cell. These results are in consistence with the previous literatures.[15,17]

2. Co-dimer adsorbed graphene

For the cobalt dimer adsorption, both PBE and LDA calculations yield consistent results that the dimer takes C_v configuration. However, in PBE calculations, the A_v, B_v, A_h, and C_h configurations are unstable; while in LDA calculations, only the B_v configuration is unstable. The adsorption energy E_{ad} also indicates a weaker binding between the dimer and graphene in PBE calculation than in LDA calculation. Since both PBE and LDA calculations produce the same stable configuration, they also yield quite similar electronic structure. Therefore we only report and discuss the PBE results in further detail.

The majority spin channel of the cobalt dimer adsorbed graphene shows an energy gap of ≈0.3 eV, and its minority spin channel is gapless (Fig. 5). However, the PDOS analysis

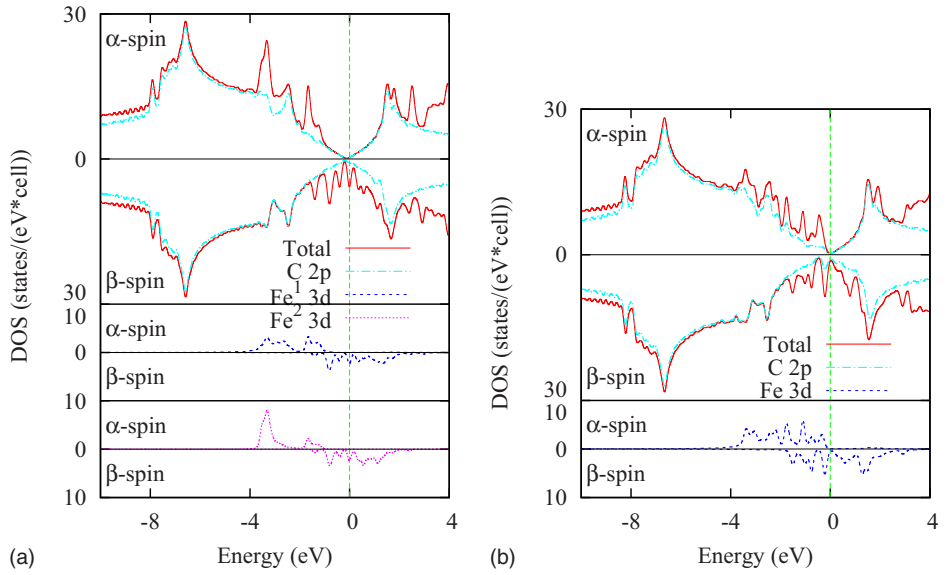

FIG. 4. (Color online) Fe-dimer adsorbed graphene DOS projected onto atomic orbitals. (a) PBE result: the solid line in the upper subfigure is the total DOS; the dot-dashed line in the upper subfigure is the PDOS on C $2p$ orbitals; the dashed line in the middle subfigure is the PDOS on the Fe^1 $3d$ orbitals; the dotted line in the bottom subfigure is the PDOS on the Fe^2 $3d$ orbitals. In each subfigure, the upper panel represents the majority (α) spin; the lower panel the minority (β) spin. (b) LDA result: the solid line in the upper subfigure is the total DOS; the dot-dashed line in the upper subfigure is the PDOS on C $2p$ orbitals; the dashed line in the lower subfigure is the PDOS on the Fe $3d$ orbitals. Since the two Fe atoms are equivalent in LDA result, only the summed PDOS of Fe $3d$ orbitals are presented.

shows that the DOS within approximately $E_F-0.3$ eV to $E_F+0.3$ eV are dominated by the cobalt atom away from the graphene layer (Co^2). These states are primarily localized around the Co^2, and do not contribute to the electronic transport process. The $3d$ orbitals of the cobalt atom directly bonded with the graphene layer (Co^1) and the C $2p$ orbitals hybridize from $E_F-2.0$ eV to $E_F+1.0$ eV for the minority spin and from $E_F-2.0$ eV to $E_F+1.0$ eV for the majority spin. Most of the states between $E_F+1.2$ eV and $E_F+2.0$ eV are from C $2p$ orbitals for both the majority and the minority spins.

TABLE IV. The local charge (n_M,$n_{M'}$), the magnetic moment (m_M,$m_{M'}$), and their projected value on $3d$ orbitals on individual metal atoms of the dimer adsorbed on graphene. For the S_h configurations, the two atoms are equivalent, thus only one number is listed for each column; for the S_v configurations, the numbers for the metal atom directly binded to the graphene layer (M) are listed outside the parenthesis, and the numbers for the other atom (M') are inside the parenthesis.

Atom	n_M (e)	$n_{M\,3d}$ (e)	m_M (μ_B)	$m_{M\,3d}$ (μ_B)
Fe (PBE, C_v)	7.67(8.09)	6.96(6.72)	2.76(3.28)	2.78(3.19)
Fe (LDA, B_h)	7.66	6.94	2.99	2.64
Co (PBE, C_v)	8.56(9.02)	7.94(7.58)	1.58(2.46)	1.65(2.37)
Co (LDA, C_v)	8.64(9.05)	8.02(7.60)	1.49(2.40)	1.53(2.35)
Ni (PBE, C_v)	9.52(10.25)	8.82(8.85)	0.77(1.15)	0.82(1.11)
Ni (LDA, C_h)	9.37	9.04	0.00	0.00
Cu (PBE, B_v)	10.67(11.17)	9.79(9.95)	0.00(0.00)	0.00(0.00)
Cu (LDA, B_v)	10.62(11.17)	9.74(9.93)	0.00(0.00)	0.00(0.00)

The Löwdin's charge analysis shows that the Co^1 atom loses $\approx$0.4 electrons while the Co^2 atom remains almost neutral. Due to the orbital hybridizations, the Co^1 and Co^2 atoms possess $\approx$8.0 and 7.6 electrons, respectively. Each cobalt atom thus yields approximately two unpaired electrons and

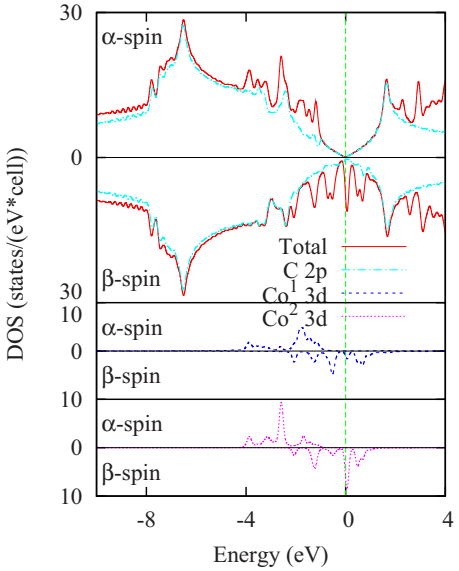

FIG. 5. (Color online) Co-dimer adsorbed graphene DOS projected onto atomic orbitals (PBE result). The solid line in the upper subfigure is the total DOS; the dot-dashed line in the upper subfigure is the PDOS on C $2p$ orbitals; the dashed line in the middle subfigure is the PDOS on the Co^1 $3d$ orbitals; the dotted line in the bottom subfigure is the PDOS on the Co^2 $3d$ orbitals. In each subfigure, the upper panel represents the majority (α) spin; the lower panel the minority (β) spin.

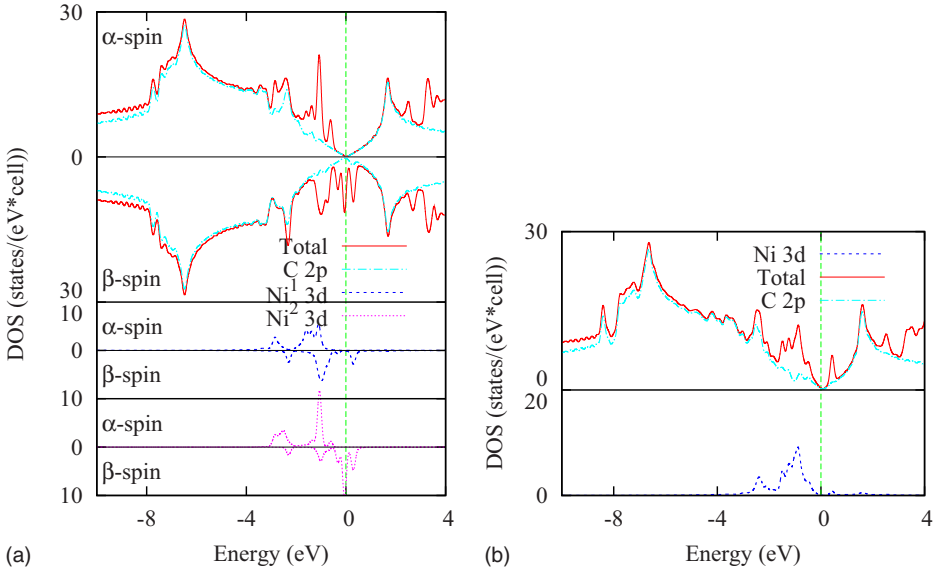

FIG. 6. (Color online) Ni-dimer adsorbed graphene DOS projected onto atomic orbitals. (a) PBE result: the solid line in the upper subfigure is the total DOS; the dot-dashed line in the upper subfigure is the PDOS on C $2p$ orbitals; the dashed line in the middle subfigure is the PDOS on the Ni^1 $3d$ orbitals; the dotted line in the bottom subfigure is the PDOS on the Ni^2 $3d$ orbitals. The α spin obviously differs from the β spin, showing that the system possesses local magnetism. (b) LDA result: the solid line in the upper subfigure is the total DOS; the dot-dashed line in the upper subfigure is the PDOS on C $2p$ orbitals; the dashed line in the lower subfigure is the PDOS on the Ni $3d$ orbitals. Since the system is not spin-polarized under LDA, we show only the α-spin in our figure. Moreover, two Ni atoms are equivalent in LDA calculation, we show only the summed PDOS of Ni $3d$ orbitals.

gives a total magnetic moment of $\approx 4\ \mu_B$/cell. This result is also in consistency with the isolated cobalt dimer calculation, since the Co-Co bond length variation is less than 5%.

3. Ni-dimer adsorbed graphene

For the nickel dimer adsorbed graphene, the PBE and LDA calculations yield completely different results. In the PBE calculations, the nickel dimer vertically binds to the hex-center site, forming a C_v configuration with a magnetic moment of $2.04\mu_B$/dimer. In the LDA calculations, the nickel dimer atoms binds to two neighboring hex-center sites, forming a C_h configuration with no spin polarization. By closer examination, one can see that the nickel atoms form surprisingly strong bindings with the graphene layer in the LDA calculations (as shown by the binding energy $E_b = 2.53$ eV), and therefore the Ni-Ni bond is much weakened after the adsorption (the bond length changes $\approx 15\%$). The much weakened bond length suggests that the dimer behaves like two adjacent adatoms under LDA after adsorption, thus the dimer does not show any magnetism. The binding between the nickel dimer and the graphene layer is much weaker in the PBE calculations ($E_b = 0.92$ eV), and the bond length change is much smaller ($\approx 3\%$). Therefore the adsorbed dimer also shows $\approx 2.04\mu_B$ magnetic moment under PBE like an isolated nickel dimer.

We show in Fig. 6 the DOS and PDOS results of the most stable nickel dimer adsorbed graphene configurations under LDA (C_h) and PBE (C_v). Similar to the iron-dimer adsorption case, the difference between the LDA and the PBE results are primarily due to the different stable configurations, and both functionals would yield similar results if the same configuration were used in the calculations. Under LDA, the nickel dimer adsorbed graphene is a semiconductor with an energy gap of ≈ 0.3 eV. As we discussed earlier, the nickel dimer atoms behave similar to the nickel adatom adsorbed on graphene under LDA, which is also indicated by the transferred charge (Table IV). The PDOS (LDA) calculations show that the states above E_F are dominated by the C $2p$ orbitals, except for the first large DOS peak around $E_F + 0.5$ eV which is primarily contributed by the Ni $4s$ orbitals; and the C $2p$ orbitals strongly hybridize with the Ni $3d$ orbitals within approximately $E_F - 2.0$ eV to E_F. Under PBE, the nickel dimer adsorbed graphene shows a band gap of ≈ 0.3 eV in its majority spin DOS and no band gap in its minority spin DOS (Fig. 7). However, the PDOS (PBE) calculation shows that the minority spin DOS within $E_F - 0.1$ to $E_F + 0.1$ is dominated by $3d$ orbitals of the Ni^2 atom, which does not directly bind to graphene. The Ni^2 $3d$ orbitals are quite localized, therefore do not contribute to electron transport process. The C $2p$ orbitals strongly hybridize with the Ni^1 $3d$ orbitals from $E_F - 2.0$ eV to $E_F - 0.5$ eV for the majority spin, and from $E_F - 1.5$ eV to $E_F - 0.5$ eV for the minority spin.

4. Cu-dimer adsorbed graphene

For the copper dimers, the binding between the Cu atom and the graphene layer is too weak (Table I), thus the dimer binds with the graphene layer through one of the atoms (B_v configuration), and the dimer bond length variation is less than 3%. Under LDA, the adsorption of copper is assisted by copper dimerization, since the copper dimer adsorption energy (1.08 eV/dimer) is larger than the copper adatom adsorption energy (0.85 eV/dimer); while under PBE, the adsorption energy of copper dimer (0.43 eV) is almost the same

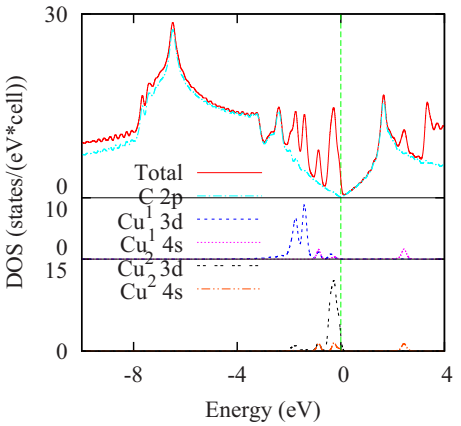

FIG. 7. (Color online) Cu-dimer adsorbed graphene DOS projected onto atomic orbitals. The subfigures from top to bottom are "Total," "Cu^1," and "Cu^2," respectively. The solid line in the top subfigure is the total DOS; the dash-dotted line in the top subfigure is the PDOS on the C $2p$ orbitals; the dashed line in the middle subfigure is the PDOS on the $3d$ orbitals of the Cu atom close to the graphene layer (Cu^1 atom); the dotted line in the middle subfigure is the PDOS on the $4s$ orbitals of the Cu^1 atom; the double-dotted line in the bottom subfigure is the PDOS on the $3d$ orbitals of the other Cu atom (Cu^2 atom); and the dash-double-dotted line in the bottom subfigure is the PDOS on the $4s$ orbitals of the Cu^2 atom. Since the system is not spin-polarized, we show only the α spin in our figure.

as the copper adatom (0.44 eV). For all other species (Fe, Co, Ni) the dimer adsorption energy is always significantly less than the adatom adsorption energy in both calculations. In both PBE and LDA calculations, the copper dimer A_v configuration energy is very close to its most stable B_v configuration energy (only 31 meV/5 meV higher in the PBE/LDA calculation), indicating that the dimer can freely move along the C-C bonds under ambient conditions. Similar to the cobalt dimer adsorbed system, both PBE and LDA calculations yield consistent DOS results, and thus we only present and discuss the PBE results in detail.

The DOS of copper dimer adsorbed graphene shows no gap and the system is therefore a metal. The PDOS analysis shows that the states above $E_F+0.1$ eV are exclusively contributed by the C $2p$ orbitals, and the states between approximately $E_F-0.6$ eV and $E_F+0.1$ eV are dominated by the $3d$ orbitals of the copper atom away from the graphene layer (Cu^2). This is similar to the cobalt dimer adsorbed graphene where the states close to E_F are dominated by the Co^2 atom. The Cu^1 $3d$ and C $2p$ orbital-hybridization takes place below $E_F-1.0$ eV. The Löwdin's charge analysis (Table IV) indicates that the $3d$ orbitals of both Cu atoms are very close to full shell, and the $4s$ orbitals hybridize to form the Cu-Cu bond, thus the system is nonmagnetic. The charge analysis also shows that the Cu^2 atom obtains $0.17e$ electron from Cu^1 atom. Therefore, the Cu^1 atom becomes more electron deficient and thus the Cu^1-C bonds are strengthened. This explains why the copper dimer adsorption energy is close to or even larger than its adatom adsorption energy.

IV. CONCLUSION

In summary, we have performed DFT calculations on transition metal (Fe, Co, Ni, and Cu) adatom and dimer adsorbed graphenes, and studied their geometric properties, electronic structure, and magnetism. For the adatom adsorption, both PBE and LDA calculations yield the same results, that the iron, cobalt, and nickel adatom chemisorb on the hex-center site; while the copper adatom physisorbs on the bond-center site. For the dimer adsorption, PBE and LDA calculations yield consistent results only for the cobalt dimer, who chemisorbs on C_v site, and the copper dimer, who physisorbs on B_v site. PBE calculations indicate that iron dimer and nickel dimer adsorption take distorted C_v configuration and C_v configuration, respectively; while LDA calculations suggest that they take B_h and C_h configurations, respectively. With iron and cobalt adatom adsorption, graphene becomes a half-metal which can be used as a spin-filtering material. The iron-dimer adsorbed graphene is also a half-metal, but the cobalt dimer adsorbed graphene is not. The nickel adatom adsorbed graphene is nonmagnetic and semiconducting, but PBE and LDA calculations yield controversial results over the magnetic and transport properties of the nickel dimer adsorbed graphene. The copper adatom exhibits $1\mu_B$ local magnetic moment while the copper dimer does not show any magnetism. The adsorption energy indicates the copper dimer can barrierlessly diffuse along the graphene C-C bonds. These results show that the graphene properties can be effectively modulated by transition metal adsorption, and that the transition metal adsorbed graphene can serve as potential materials in nanoelectronics, spintronics, or electrochemistry.

ACKNOWLEDGMENTS

The authors would like to thank National Science Foundation of China (NSFC) (Grant No. 10904127), as well as the Shanghai Supercomputing Center (SSC) for the computational support.

*ccao@hznu.edu.cn

[1] K. S. Novoselov, A. K. Geim, S. V. Morozov, D. Jiang, Y. Zhang, S. V. Dubonos, I. V. Grigorieva, and A. A. Firsov, Science **306**, 666 (2004).
[2] M. S. Dresselhaus and G. Dresselhaus, Adv. Phys. **51**, 1 (2002).
[3] A. Hashimoto, K. Suenaga, A. Gloter, and K. Urita, Nature (London) **430**, 870 (2004).
[4] Y. W. Son, M. L. Cohen, and S. G. Louie, Nature (London) **444**, 347 (2006).
[5] Y. W. Son, M. L. Cohen, and S. G. Louie, Phys. Rev. Lett. **97**, 216803 (2006).
[6] J. R. Williams, L. DiCarlo, and C. M. Marcus, Science **317**, 638 (2007).
[7] D. A. Abanin and L. S. Levitov, Science **317**, 641 (2007).

[8] E. H. Hwang, S. Adam, and S. D. Sarma, Phys. Rev. B **76**, 195421 (2007).
[9] F. Schedin, A. K. Geim, S. V. Morozov, E. W. Hill, P. Blake, M. I. Katsnelson, and K. S. Novoselov, Nature Mater. **6**, 652 (2007).
[10] B. Huang, Z. Li, Z. Liu, G. Zhou, S. Hao, J. Wu, B.-L. Gu, and W. Duan, J. Phys. Chem. C **112**, 13442 (2008).
[11] Q. J. Wang and J. G. Che, Phys. Rev. Lett. **103**, 066802 (2009).
[12] M. Vanin, J. J. Mortensen, A. K. Kelkkanen, J. M. Garcia-Lastra, K. S. Thygesen, and K. W. Jacobsen, Phys. Rev. B **81**, 081408 (2010).
[13] P. A. Khomyakov, G. Giovannetti, P. C. Rusu, G. Brocks, J. van den Brink, and P. J. Kelly, Phys. Rev. B **79**, 195425 (2009).
[14] V. M. Karpan, P. A. Khomyakov, A. A. Starikov, G. Giovannetti, M. Zwierzycki, M. Talanana, G. Brocks, J. van den Brink, and P. J. Kelly, Phys. Rev. B **78**, 195419 (2008).
[15] D. M. Duffy and J. A. Blackman, Phys. Rev. B **58**, 7443 (1998).
[16] K. T. Chan, J. B. Neaton, and M. L. Cohen, Phys. Rev. B **77**, 235430 (2008).
[17] H. Johll and H. C. Kang, Phys. Rev. B **79**, 245416 (2009).
[18] M. Wu, E.-Z. Liu, M.-Y. Ge, and J. Z. Jiang, Appl. Phys. Lett. **94**, 102505 (2009).
[19] T. O. Wehling, A. V. Balatsky, M. I. Katsnelson, A. I. Lichtenstein, and A. Rosch, Phys. Rev. B **81**, 115427 (2010).
[20] R. C. Longo, J. Carrete, J. Ferrer, and L. J. Gallego, Phys. Rev. B **81**, 115418 (2010).
[21] V. A. Rigo, T. B. Martins, A. J. R. da Silva, A. Fazzio, and R. H. Miwa, Phys. Rev. B **79**, 075435 (2009).
[22] H. Sevinçli, M. Topsakal, E. Durgun, and S. Ciraci, Phys. Rev. B **77**, 195434 (2008).
[23] O. Üzengi Aktürk and M. Tomak, Phys. Rev. B **80**, 085417 (2009).
[24] Y. Sanchez-Paisal, D. Sanchez-Portal, and A. Ayuela, Phys. Rev. B **80**, 045428 (2009).
[25] W. I. Choi, S.-H. Jhi, K. Kim, and Y.-H. Kim, Phys. Rev. B **81**, 085441 (2010).
[26] P. Krüger, A. Rakotomahevitra, J. C. Parlebas, and C. Demangeat, Phys. Rev. B **57**, 5276 (1998).
[27] M. Bäumer, J. Libuda, and H. J. Freund, Surf. Sci. **327**, 321 (1995).
[28] QUANTUM-ESPRESSO is a community project for high-quality quantum-simulation software, based on density-functional theory, and coordinated by Paolo Giannozzi. See http://www.quantum-espresso.org and http://www.pwscf.org
[29] We used the pseudopotentials c.pz-rrkjus.upf (c.pbe-rrkjus.upf), fe.pz-nd-rrkjus.upf (fe.pbe-nd-rrkjus.upf), co.pz-nd-rrkjus.upf (co.pbe-nd-rrkjus.upf), ni.pz-nd-rrkjus.upf (ni.pbe-nd-rrkjus.upf), and cu.pz-d-rrkjus.upf (cu.pbe-d-rrkjus.upf) from the http://www.quantum-espresso.org distribution for LDA (PBE) calculations.
[30] J. P. Perdew and A. Zunger, Phys. Rev. B **23**, 5048 (1981).
[31] J. P. Perdew, K. Burke, and M. Ernzerhof, Phys. Rev. Lett. **77**, 3865 (1996).
[32] Y. Yagi, T. M. Briere, M. H. F. Sluiter, V. Kumar, A. A. Farajian, and Y. Kawazoe, Phys. Rev. B **69**, 075414 (2004).
[33] C. Jozsa, M. Popinciuc, N. Tombros, H. T. Jonkman, and B. J. van Wees, Phys. Rev. B **79**, 081402 (2009).